RESEARCH ARTICLE

Linear Parameter-Varying Model Predictive Control for Intelligent Energy Management in Battery/Supercapacitor Electric Vehicles

MORTEZA REZAEI LARIJANI[1,2], (Student Member, IEEE),
SHAHIN HEDAYATI KIA[2], **MOHAMMADREZA ZOLGHADRI**[1], (Senior Member, IEEE),
AHMED EL HAJJAJI[2], AND **AMIR TAGHAVIPOUR**[3]

[1]Department of Electrical Engineering, Sharif University of Technology, Tehran 14588-89694, Iran
[2]Modeling, Information and Systems (MIS) Laboratory, Université de Picardie Jules Verne, 80039 Amiens, France
[3]Mechanical Engineering Department, K. N. Toosi University, Tehran 19919-43344, Iran

Corresponding author: Shahin Hedayati Kia (shdkia@u-picardie.fr)

ABSTRACT This paper presents a supervisory control strategy to intelligently split power within a hybrid energy storage system (HESS) of battery and supercapacitor (SC) in electric vehicles (EVs). The intelligent energy management strategy (IEMS) is based on linear parameter-varying model predictive control (LPV-MPC) with the main aim of mitigating battery degradation. The battery RC model is considered in the control-oriented model, where the increment of the battery current is selected as the control variable, resulting in a linear state-space model dependent on the HESS parameters, namely, the battery state-of-charge (SoC) and SC state-of-voltage (SoV). The cost function minimizes the power loss in the battery and squared error of the SoV across the prediction horizon. A new SoV control strategy is proposed based on the upcoming acceleration, providing opportunities for the efficient utilization of the SC and extending the battery lifespan. Constrained optimization is transformed into a quadratic programming problem, which can be easily solved in real time. The superiority of the proposed method in assessing battery degradation was verified by comparing different strategies using five evaluation factors under two drive cycles. Compared with the LPV-MPC, where SoV remained fixed, the proposed method demonstrates reductions of up to 18.82% in the battery current root-mean-square, 30.26% and 25.85% in the discharge and charge peak current, 9.71% in the ampere-hour throughput, 4.78% in the capacity loss, and 29.06% in the energy loss. To validate the real time performance of the proposed method, it is implemented in the real-time digital simulator (RTDS).

INDEX TERMS Batteries, electric vehicle, energy management, hybrid energy storage system, linear systems, model predictive control, quadratic programming, real-time simulation, supercapacitors.

NOMENCLATURE

DP	Dynamic Programming.
EM	Electric Motor.
EMS	Energy Management Stratgey.
EV	Electric Vehicle.
FE	Forward Euler.
HESS	Hybrid Energy Storage System.
IEMS	Intelligent Energy Management Stratgey.
LMO	Lithium Manganese Oxide.
LPV-MPC	Linear Parameter-Varying Model Predictive Control.
LTI	Linear Time-Invariant.
NCA	Lithium Nickel-Cobalt-Aluminum Oxide.
NiMH	Nickel-Metal Hydride.
OCV	Open-Circuit Voltage.
PMP	Pontryagin's Minimum Principle.
QP	Quadratic Programming.
RMS	Root Mean Square.
RMSPE	Root Mean Square Percentage Error.

The associate editor coordinating the review of this manuscript and approving it for publication was Jie Gao.

RTDS	Real-Time Digital Simulator.
RWD	Rear-Wheel Drive.
SC	Supercapacitor.
SoC	State-of-Charge.
SoV	State-of-Voltage.
UDDS	Urban Dynamometer Driving Schedule.
V2I	Vehicle-to-Infrastructure.
V2V	Vehicle-to-Vehicle.
WLTC	Worldwide Harmonized Light Vehicles Test Cycle.

I. INTRODUCTION

Electric vehicles (EVs) with hybrid energy storage system (HESS), including the battery and supercapacitor (SC), are widely recognized as a viable alternative to conventional vehicles owing to their increased efficiency, reduced noise levels, and capacity to contribute to a less polluted environment [1], [2], [3]. With its high energy density, the battery serves as the primary energy storage, whereas the SC, with its high power density, provides or captures peak power during high acceleration or braking in EVs [4], [5], [6]. Large fluctuations in power demand result in more frequent battery discharging and charging, which degrades performance and reduces lifespan [7]. This cycling event occurs more frequently in battery/SC EVs, where the battery operates within a wide range of state-of-charge (SoC) [8]. The integration of SC and employing a suitable supervisory controller not only mitigates stress on the battery and extends its lifespan but also considerably enhances the driving range of the EV, which paves the way for sustainable transportation [9]. The battery can take advantage of the HESS when coupled with a suitable supervisory controller; otherwise, improper hybridization might yield undesirable results [10]. The energy management strategy (EMS), as a supervisory controller, facilitates the practical implementation of hybridization by splitting the power flow within the HESS while considering predefined objectives and constraints [11], [12]. EMSs in EVs can be broadly classified into two main categories: rule-based and optimization-based EMSs. Rule-based EMSs can be categorized into deterministic rule-based [13], [14], fuzzy logic-based [15], [16], filter-based [17], [18], and their combinations [19], [20]. Rule-based EMSs use a set of rules derived from human experience and are suitable for implementation in a real-time digital simulator (RTDS). However, they cannot provide an optimal solution for all conditions because they require specific rules for each scenario. By contrast, optimization-based EMSs, which can be classified into global and real-time strategies, aim to solve an optimal control problem by minimizing the cost function. This cost function in a battery/SC EV aims to reduce fluctuations in the battery current and extend its lifespan [21]. As a global optimization-based EMS, dynamic programming (DP) is a commonly used algorithm that computes globally optimal solutions by decomposing the control problem into sub-problems. DP solves optimization backward but relies on knowing the entire speed drive cycle a priori [22]. Because of its requirement for recursively finding optimal solutions and the significant computational burden involved, DP is typically employed offline as a benchmark for evaluating and adjusting other control strategies [23], [24].

Real-time optimization-based EMSs provide sub-optimal solutions through the online minimization of a cost function [11]. Pontryagin's minimum principle (PMP), which is based on Hamiltonian equations, is typically considered an offline method but can also be adapted for real-time application. Nguyen et al. [25] proposed an alternative PMP for a battery/SC EV, in which the EMS dealt with a nonlinear system. To alleviate the computational burden, a simplified model was applied to the battery and SC, and the converter efficiency was kept constant to prevent switching behavior. The open-circuit voltage (OCV) of the battery cell model was assumed to be constant. However, this assumption results in deviations from the optimal solution, as, in practice, the OCV is a function of its SoC. Similarly, Odiem et al. [26] computed the optimal solution using DP and PMP offline for an electric bus with the energy storage of fuel cell, battery, and SC. Power management is then applied using a genetic algorithm, where the models of both the battery and SC are greatly simplified. Additionally, global optimality cannot be guaranteed in the PMP [27]. Furthermore, in a complicated nonlinear system, determining the co-state of the Lagrange multiplier is challenging.

In addition to the thorough modeling of the HESS, achieving optimum performance in the EMS requires information about the upcoming speed of the EV. This information can be provided through the traffic model of a connected EV using vehicle-to-vehicle (V2V) and vehicle-to-infrastructure (V2I) communications [22]. Model predictive control (MPC), as a real-time optimization-based strategy, can consider the anticipated power demand given the upcoming speed, while minimizing a cost function over the prediction horizon. As Ostadian stated [11], the EMS can be classified as an intelligent energy management strategy (IEMS) if it is implementable in the RTDS, adaptable to new environments, and capable of anticipating outputs based on the system's prediction model. All these characteristics can be integrated into an MPC method, rendering it a desirable supervisory controller for energy management in EVs [28], [29], [30], [31], [32], [33], [34]. In this respect, Xu and Shen [28] developed an MPC-based optimization strategy to efficiently split the power between the battery and engine in a connected hybrid EV. Qi et al. [29] proposed an MPC-based EMS for fuel cell/battery HESS. Liu et al. [30] proposed a model predictive current control in a DC microgrid with a battery/SC HESS. The proposed EMS mainly focuses on the voltage stability of the DC-bus and only defines the reference power, which is split by a simple low-pass filter between the battery and the SC. Golchoubian and Azad [31] developed a nonlinear MPC for an optimal power split in a battery/SC HESS. One of the challenging issues of nonlinear MPC is its implementation in RTDS owing to

the increased computational burden in solving a nonlinear system [35]. Unlike [25] and [31], where the power flows were used as control variables, Hredzak et al. [32] used explicit MPC where the currents were employed as control variables, resulting in a linear time-invariant (LTI) state-space model for the HESS. The explicit MPC computes the control action offline based on a specific scenario. Furthermore, in these studies [31], [32], a simple model was used to represent the HESS, where the battery was depicted as a voltage source with a constant OCV and a resistor, neither of which was dependent on the SoC. However, there are more sophisticated RC models that can accurately capture the dynamic behavior of Lithium-ion (Li-ion) cells in EV applications. Zhou et al. [36] developed an adaptive MPC for HESS, which solves the quadratic programming (QP) problem. This indicates that the adaptive MPC outperformed the LTI-MPC. However, because the power flow is utilized as the control action, the model is nonlinear and needs to be linearized around the operating point. In this regard, Jia et al. [34] considered dynamic models of the battery and developed a linear parameter-varying (LPV) prediction model, where the control variables are the SC current and the increment of the battery current. Linear parameter-varying model predictive control (LPV-MPC) strategy is used to solve the constrained QP problem in real time. The results demonstrate that the use of LPV-MPC leads to significantly higher accuracy compared to LTI-MPC and effectively reduces battery energy loss. However, the state-of-voltage (SoV) of the SC remained constant (SoV=0.75), thereby hindering efficient utilization of the SC. Moreover, incorporating the minimization of both SC and battery power losses into the cost function might not be reasonable. In addition, the proposed EMS is a frozen-time MPC, where the power demand is considered as a constant measured disturbance over the entire prediction horizon [37]. This type of formulation is unsuitable for urban drive cycles, particularly when the speed changes frequently, which may substantially degrade the performance of the EMS [38].

In this paper, the LPV model of the HESS is developed as a predictive model based on the dynamic RC model of the battery, which is more accurate than the static one [39]. The state-space model depends on the HESS parameters, including the resistance, capacitance, voltage, and SoC of the battery, SoV of the SC, and efficiency factors in the charging and discharging modes of the bi-directional dc-dc converter. The state-space matrices are updated at each time-step; however, they remain constant over the prediction horizon. The control problem is transformed into an inequality-constrained QP optimization problem, whereas the proposed LPV-MPC-based IEMS determines the optimal control action by minimizing the cost function. This cost function addresses both the power loss in the battery and control of the SoV across the prediction horizon. Furthermore, the power demand is considered as a measured disturbance, which can be computed for the next time-step using knowledge of the upcoming speed and the EV

powertrain model. It is assumed that this speed is provided by another subsystem, considering the traffic model, and V2V and V2I communications. The reference of SoV is set to the maximum SoV of the SC which is 1. However, the weighting factor of the cost function related to SoV is either 1 or 0, according to the anticipated acceleration of the EV. It is demonstrated that employing a variable SoV control strategy and considering the anticipated power demand offer tremendous potential for minimizing fluctuations in the battery current and expanding its operational lifespan. The control variable is exclusively the increment of the battery current, resulting in the QP optimization problem which includes only inequality constraints and is easily solved by conventional solvers in real time. To generate more realistic results and observe the desirable performance of the proposed IEMS, the electrochemical model of the battery pack in MapleSim is used as a representation of a real battery. Finally, the LPV-MPC-based IEMS is validated by implementation in dSPACE. Furthermore, to evaluate the performance of the proposed method, it was compared with other advanced EMSs, based on measuring 1-the root mean square (RMS) of the battery current, 2-the peak current, 3-the ampere-hour throughput, 4-the battery cell capacity loss, and 5-the battery pack energy loss, which are important factors in assessing battery degradation in EV applications [10], [33], [34], [40], [41], [42]. It is demonstrated that considering the EV's upcoming acceleration enhances the performance of the LPV-MPC in reducing battery degradation compared to other EMSs. The main contributions of this study are summarized as follows:

1) Compared to previous studies [31], [32], [43], which maintains SoV at 0.75, in this study, control of the SoV is based on the anticipated acceleration of the EV by adjusting the weighting factor. The new SoV control strategy further reduces battery current fluctuations, capacity loss, and energy loss, thereby improving battery lifetime efficiency. Also, this strategy is applicable to connected EVs, where the vehicle's upcoming speed is provided by V2V and V2I communications.

2) Using the increment of the battery current as a control action leads to a linear equation that omits the need for a nonlinear optimization method. The obtained QP optimization problem is solved using LPV-MPC, which is more accurate than LTI-MPC [32], and it does not have the complexity of nonlinear MPC.

3) A straightforward procedure for real-time modeling of a battery/SC EV, considering the efficiency factors of bidirectional dc-dc converters in charge and discharge modes, has been developed [44], [45]. The proposed framework can be used to evaluate different EMSs in real time.

The structure of the paper is as follows. Section II explains the configuration of the HESS consisting of the battery and SC, along with its modeling. In Section III, the LPV-MPC-based IEMS is proposed, involving the obtained LPV model of the HESS, formulation of the QP optimization problem, and
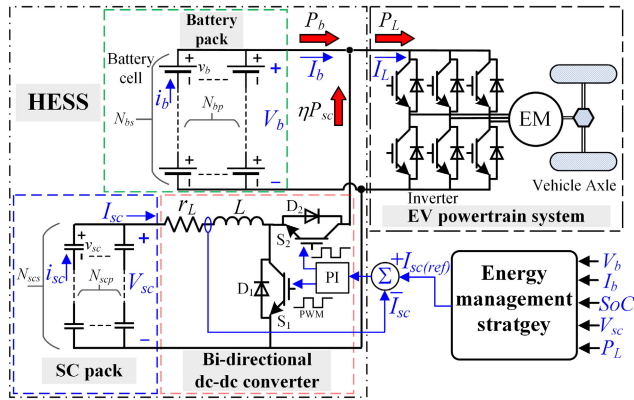
FIGURE 1. HESS of battery/SC EV in the semi-active topology.

FIGURE 2. Double RC branch model of the battery cell [44].

FIGURE 3. Block diagram of the battery pack model for the simulation.

proposing the SoV control strategy based on the upcoming acceleration. Section IV focuses on the real-time validation of the proposed EMS, analyzes the results, and compares them with those of other approaches. Finally, the conclusions are provided in Section V.

II. HESS CONFIGURATION AND MODELING

As a compromise between control performance, weight, reliability, and cost, the semi-active topology is better suited for configuring the HESS of the battery and SC [40], [46], [47]. In the most commonly used type of semi-active topology, depicted in Fig. 1, the battery pack is directly linked to the inverter, ensuring a stable voltage at the electric motor (EM) drive, and the SC pack acts as an auxiliary power supply, which is connected to the battery pack via a bidirectional dc-dc converter. The converter adjusts the current of the SC pack to match the reference current provided by the supervisory controller. The proposed supervisory controller is based on MPC, which aims to split the power flow between the battery pack and SC pack. Since the accuracy of the system model is pivotal for the optimal performance of MPC, dynamic models of the battery and SC are utilized, and the converter efficiency factors in both the charging and discharging modes are considered.

A. BATTERY

Li-ion batteries are the main components of EVs and play a crucial role in their performance. The OCV of the majority of Li-ion batteries commonly used in EV applications varies widely over SoC, including lithium nickel-cobalt-aluminum oxide (NCA), lithium manganese oxide (LMO), and nickel-metal hydride (NiMH) batteries [42], [44], [48], [49]. Therefore, it is crucial to place more emphasis on accurately modeling battery cells. Battery cell behaviors can be represented by electrochemical, data-driven, and equivalent circuit models [50]. Equivalent circuit models are suitable for model-based controllers as they represent the battery cell using electrical elements, such as voltage sources, resistors, and capacitors. These models include the single RC branch model, double RC branch model, and triple RC branch model, among which the double RC branch model is accurate
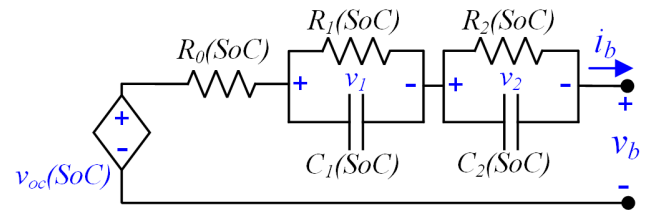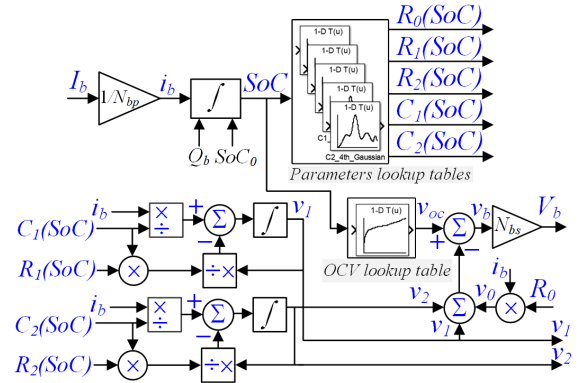
enough to capture the dynamic behavior of the battery cell and can be effectively utilized as a control-oriented model in LPV-MPC [39], [49], [50], [51], [52], [53]. In Fig. 2, a double RC model of the battery cell is illustrated, of which the parameters depend on the SoC and are influenced by the battery current. Here, v_{oc} represents OCV, R_0 denotes the resistance for modeling the voltage drop, and v_1 and v_2 are the voltages of R_1C_1 and R_2C_2 branches, respectively. These branches exhibit the effects of the electrode surface and diffusion process, which exhibit slow and fast dynamics, respectively. The battery cell SoC, which defines the amount of battery charge, is calculated by the Coulomb-counting method, as given in (1).

$$\frac{d}{dt}SoC(t) = \frac{-I_b(t)}{N_{bp}Q_b} \quad (1)$$

where Q_b is the battery cell rated capacity in ampere-seconds, I_b is the battery pack current, which is equal to the battery cell current (i_b) multiplied by the number of parallel cells (N_{bp}). The terminal and the RC branch voltages are described in (2) and (3), respectively.

$$v_b(t) = v_{oc} - R_0 i_b(t) - v_1(t) - v_2(t) \quad (2)$$

$$C_x \frac{dv_x(t)}{dt} + \frac{v_x(t)}{R_x} = i_b(t), \quad x \in \{1, 2\} \quad (3)$$

The battery pack terminal voltage V_b, is determined by multiplying the cell voltage v_b, by the total number of battery cells in series N_{bs}. The OCV and RC parameters are computed by the discharge pulse current and stored in lookup tables, whose input is the SoC [44]. A block diagram of the battery pack model used for the simulation is shown in Fig. 3.
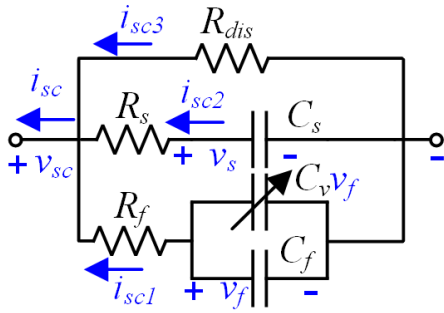
FIGURE 4. Faranda model of the supercapacitor cell [54].

FIGURE 5. Block diagram of the SC pack model for the simulation.

B. SUPERCAPACITOR

There are various models for representing SC, such as the first-order model, Zubeita model, RC transmission line model, and Faranda model [54], [55], [56], [57]. The widely used model is the Faranda model, which represents the dynamic behavior of SCs in EV applications. This model incorporates an equivalent circuit that includes two RC branches with a voltage-dependent capacitance, as shown in Fig. 4. The dynamic equations of the SC cell model are presented in (4).

$$i_{sc}(t) = i_{sc1}(t) + i_{sc2}(t) + i_{sc3}(t) \tag{4a}$$

$$v_{sc}(t) = -R_f i_{sc1}(t) + v_f(t) \tag{4b}$$

$$v_{sc}(t) = -R_s i_{sc2}(t) + v_s(t) \tag{4c}$$

$$v_{sc}(t) = -R_{dis} i_{sc3}(t) \tag{4d}$$

$$i_{sc1}(t) = -\frac{d}{dt}\left((C_v v_f(t) + C_f)v_f(t)\right)$$
$$\rightarrow v_f(t) = v_f(t_0) - \int_{t_0}^{t} \frac{i_{sc1}(t)}{(2C_v v_f(t) + C_f)} dt \tag{4e}$$

$$i_{sc2}(t) = -C_s \frac{dv_s(t)}{dt}$$
$$\rightarrow v_s(t) = v_s(t_0) - \frac{1}{C_s} \int_{t_0}^{t} i_{sc2}(t) dt \tag{4f}$$

where i_{sc} and v_{sc} are the current and voltage of the SC cell, respectively. The SC pack voltage V_{sc} can be computed by multiplying v_{sc} by the number of series cells N_{scs}. Given (4), a block diagram of the SC pack model for the simulation is shown in Fig. 5. For the prediction model, SoV, which is the ratio of v_{sc} to the SC cell rated voltage $v_{sc,r}$, can be obtained using (5).

$$\frac{d}{dt} SoV(t) = \frac{-I_{sc}(t)}{Q_{sc}} \tag{5}$$

where I_{sc} and Q_{sc} represent the current and capacity of the SC pack, respectively. Q_{sc} is calculated by $v_{sc,r} N_{scp} C_{sc}$, where N_{scp} is the parallel number of SC cells and C_{sc} is the SC cell rated capacitance.
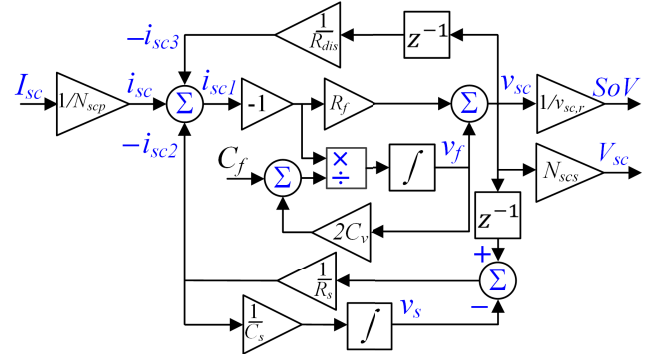
C. POWER FLOW

There is a relationship between the battery pack power, $P_b(t)$, and the SC pack power, $P_{sc}(t)$, given by (6).

$$P_L(t) = \underbrace{V_b(t)I_b(t)}_{P_b(t)} + \eta(t) \underbrace{V_{sc}(t)I_{sc}(t)}_{P_{sc}(t)} \tag{6}$$

where $P_L(t)$, is the load power or power demand, which can be computed using the EV powertrain model presented in [45]. The efficiency of the bi-directional dc-dc converter is given by (7).

$$\eta(t) = \begin{cases} \eta_{dis}, & \text{if } I_{sc} \geq 0 \\ 1/\eta_{cha}, & \text{if } I_{sc} < 0 \end{cases} \tag{7}$$

where η_{dis} and η_{cha} are the efficiency factors of the bi-directional dc-dc converter during discharge (acceleration), $I_{sc} \geq 0$, and charge (braking), $I_{sc} < 0$, defined in (8) and (9), respectively [45].

$$\eta_{dis} = \frac{V_b}{V_{sc}} \left(\frac{V_{sc} - (R_{on1} + r_L)I_{sc}}{V_b + V_{D2} + (R_{D2} - R_{on1})I_{sc}} - f_{sw}(t_r + \frac{Q_r}{I_{sc}}) \right) \tag{8}$$

$$\eta_{cha} = \frac{V_{sc}}{V_b} \left(\frac{1}{\frac{V_{sc} + V_{D1} - (R_{D1} + r_L)I_{sc}}{V_b + V_{D1} + (R_{on2} - R_{D1})I_{sc}} - f_{sw}(t_r + \frac{Q_r}{|I_{sc}|})} \right) \tag{9}$$

where R_{on1} and R_{on2} are the drain-source on-resistances of switches S_1 and S_2 when they are turned on; R_{D1} and R_{D2}, as well as V_{D1} and V_{D2} are the diodes D_1 and D_2 resistances and voltages when they conduct, respectively; t_r is the diode reverse recovery time, Q_r is the diode recovered charge; and f_{sw} is the switching frequency (Fig. 1) [45].

III. PROPOSED LPV-MPC-BASED IEMS

MPC optimizes a multivariable constrained control problem by determining the control action through the prediction model by minimizing the cost function over a finite prediction horizon at each time-step [11]. Selecting the current as a control action results in a linear state-space equation as a prediction model for the HESS. However, this depends on the battery and SC parameters. In this regard, the LPV-MPC method is employed to solve the optimization problem, where the state-space matrices are updated at each time-step but remain fixed over the prediction horizon. The optimization

problem is transformed into an inequality-constrained QP optimization formulation, which is solved using Hildreth's quadratic programming algorithm in real time.

A. HESS DISCRETE EQUATION

First, the discrete equation of the HESS is obtained. For the battery model, equation (1) can be discretized through the forward Euler (FE) method, as given by (10).

$$SoC(k + 1) = SoC(k) - \frac{T}{N_{bp}Q_b}I_b(k) \qquad (10)$$

where T denotes discrete sample time. Similarly, for the voltages of the RC branches, the discrete form of (3) is given by (11).

$$v_x(k + 1)$$
$$= \left(1 - \frac{T}{R_x(SoC(k))C_x(SoC(k))}\right)v_x(k) + \frac{TI_b(k)}{N_{bp}C_x(SoC(k))}$$
$$x \in \{1, 2\} \qquad (11)$$

Similarly, for the SC, given (5), the discrete equation of the SoV is obtained through the FE method, as shown in (12).

$$SoV(k + 1) = SoV(k) - \frac{T}{Q_{sc}}I_{sc}(k) \qquad (12)$$

According to (6), the discrete form of the SC pack current can be obtained in terms of P_L and I_b as defined in (13):

$$I_{sc}(k) = \frac{P_L(k) - V_b(k)I_b(k)}{\eta(k)V_{sc}(k)} \qquad (13)$$

Additionally, by incorporating the inherent integral and accounting for the variation in the battery current within the cost function, variable I_b can be replaced by the relation provided in (14).

$$I_b(k) = I_b(k - 1) + \Delta I_b(k) \qquad (14)$$

where $\Delta I_b(k)$ is the increment of the battery current and $I_b(k - 1)$ is the current at the previous time-step. Given (13) and (14), I_{sc} is computed using $\Delta I_b(k)$ and $P_L(k)$.

Subsequently, the SoV in (12) is determined using the same parameters. Finally, with the discrete equations given in (10), (11), (12), (13), and (14); considering $SoC(k)$, $v_1(k)$, $v_2(k)$, $SoV(k)$, and $I_b(k - 1)$ as state variables; $\Delta I_b(k)$ as a control variable; and $P_L(k)$ as a measured disturbance, the state-space model of the HESS can be developed, as defined in (15), as shown at the bottom of the page. The state-space model is linear, but its matrices depend on the parameters. The numbers of state and control variables are $n_x = 5$, and $n_u = 1$, respectively. $\Delta u(k) \in \mathbb{R}^{n_u}$ is the incremental control variable, $x(k) \in \mathbb{R}^{n_x}$ is the vector of the state variables, $A(k) \in \mathbb{R}^{n_x \times n_x}$ is the system matrix, $B(k) \in \mathbb{R}^{n_x}$ is the input matrix of the control, and $B_d(k) \in \mathbb{R}^{n_x}$ is the input matrix of the disturbance. They change at each time-step, given the HESS parameters, which depend on SoC and SoV. The only control variable is the increment of the battery current, which is supposed to be calculated by the LPV-MPC at each time-step.

B. FORMULATION OF LPV-MPC

The state-space model in (15) is used as a prediction model, where $x(k + 1|k)$ represents the predicted value of x at time-step $k + 1$ according to its value at k. The future state variables vector over the prediction horizon, $X(k) = \left[x(k + 1|k), \ldots, x(k + N_p|k)\right]^T \in \mathbb{R}^{n_x N_p}$, can be computed by (16a).

$$X(k) = F(k)x(k) + \phi(k)\Delta U(k) + \phi_d(k)P_{L,ref}(k)$$
$$\in \mathbb{R}^{n_x N_p} \qquad (16a)$$

$$F(k) = \left[A(k), A^2(k), \ldots, A^{N_p}(k)\right]^T \quad \in \mathbb{R}^{n_x N_p \times n_x}$$

$$\phi(k) = \qquad (16b)$$

$$\begin{bmatrix} B(k) & 0 & \ldots & 0 \\ A(k)B(k) & B(k) & \ldots & 0 \\ A^2(k)B(k) & A(k)B(k) & \ldots & 0 \\ \vdots & \vdots & \ddots & \vdots \\ A^{N_p-1}(k)B(k) & A^{N_p-2}(k)B(k) & \ldots & A^{N_p-N_c}(k)B(k) \end{bmatrix}$$

$$\in \mathbb{R}^{n_x N_p \times n_u N_c} \qquad (16c)$$

$$x(k + 1) = \underbrace{\begin{bmatrix} 1 & 0 & 0 & 0 & -T/(N_{bp}Q_b) \\ 0 & 1 - T/(R_1(SoC(k))C_1(SoC(k))) & 0 & 0 & T/(N_{bp}C_1(SoC(k))) \\ 0 & 0 & 1 - T/(R_2(SoC(k))C_2(SoC(k))) & 0 & T/(N_{bp}C_2(SoC(k))) \\ 0 & 0 & 0 & 1 & TV_b(k)/(Q_{sc}\eta(k)V_{sc}(k)) \\ 0 & 0 & 0 & 0 & 1 \end{bmatrix}}_{A(k)} x(k)$$

$$+ \underbrace{\begin{bmatrix} -T/(N_{bp}Q_b) \\ T/(N_{bp}C_1(SoC(k))) \\ T/(N_{bp}C_2(SoC(k))) \\ TV_b(k)/(Q_{sc}\eta(k)V_{sc}(k)) \\ 1 \end{bmatrix}}_{B(k)} \Delta u(k) + \underbrace{\begin{bmatrix} 0 \\ 0 \\ 0 \\ -T/(Q_{sc}\eta(k)V_{sc}(k)) \\ 0 \end{bmatrix}}_{B_d(k)} P_L(k)$$

$$x(k) = \left[SoC(k), v_1(k), v_2(k), SoV(k), I_b(k - 1)\right]^T, \quad \Delta u(k) = \Delta I_b(k), \quad n_x = 5, n_u = 1 \qquad (15)$$

$$\phi_d(k) =$$

$$\begin{bmatrix} B_d(k) & 0 & \dots & 0 \\ A(k)B_d(k) & B_d(k) & \dots & 0 \\ A^2(k)B_d(k) & A(k)B_d(k) & \dots & 0 \\ \vdots & \vdots & \ddots & \vdots \\ A^{N_p-1}(k)B_d(k) & A^{N_p-2}(k)B_d(k) & \dots & B_d(k) \end{bmatrix}$$

$$\in \mathbb{R}^{n_x N_p \times N_p} \tag{16d}$$

The optimization at each time-step includes the increment of the control variable over the control horizon, N_c, $\Delta U(k) = \left[\Delta u(k|k), \Delta u(k+1|k), \dots, \Delta u(k+N_c-1|k) \right]^T \in \mathbb{R}^{n_u N_c}$. The state-space model is determined at each time-step based on the updated parameters of the HESS. However, the matrices remain constant over the prediction horizon, resulting in a small error but significantly reducing computational burden [58]. The matrices $F(k)$, $\phi(k)$ and $\phi_d(k)$ require parameter information only at the current time-step, k. In this study, it is assumed that the speed at the next time-step is provided through the traffic model using V2V and V2I communications. The upcoming speed at the next time-step enables straightforward computation of the power demand at the next time-step, $P_L(k+1|k)$, based on the EV powertrain model obtained in [45]. Thus, the vector $P_{L,ref}(k) = \left[P_L(k|k), P_L(k+1|k), \dots, P_L(k+N_p-1|k) \right]^T \in \mathbb{R}^{N_p}$ consists of the current state power demand, $P_L(k|k)$, and its upcoming value, $P_L(k+1|k)$, which is known. The remaining elements, $P_L(k+2|k)$ up to $P_L(k+N_p-1|k)$, are the same as $P_L(k+1|k)$. Hence, in terms of power demand, LPV-MPC is a combination of prescient and frozen-time MPC, where the disturbance is known for the next time-step and remains constant over N_p [37]. Because of the anticipation at $k+1$, N_p should be at least 2.

C. COST FUNCTION

Both instantaneous and temporal changes in the battery current significantly affect battery lifetime [59]. Moreover, the SC should be controlled to supply peak power during fast acceleration and braking modes. In this context, the cost function focuses on minimizing the battery power loss and squared error of the SoV. Hence, the cost function is given by (17).

$$L(k) = \lambda_1 f_1(k) + \lambda_2 f_2(k) + \lambda_3 f_3(k) \tag{17}$$

where λ_1 to λ_3 are the weighting factors for each objective function of f_1 to f_3 which are defined in (18a)-(18c).

$$f_1(k) = (SoV_{ref} - SoV(k))^2 \tag{18a}$$

$$f_2(k) = R_0(SoC(k))i_b^2(k) + \frac{v_1^2(k)}{R_1(SoC(k))} + \frac{v_2^2(k)}{R_2(SoC(k))} \tag{18b}$$

$$f_3(k) = \Delta I_b^2(k) \tag{18c}$$

Here, f_1 minimizes the squared error of the SoV, f_2 minimizes the battery power loss, and f_3 minimizes the battery current fluctuations over the time-step horizon.

D. OPTIMIZATION OVER THE PREDICTION HORIZON

Given (17), the LPV-MPC minimizes the predicted total cost function J, over the prediction horizon at each time-step, as defined in (19).

$$J = \sum_{i=1}^{N_p} (\lambda_1 f_1(k+i|k) + \lambda_2 f_2(k+i|k))$$

$$+ \sum_{j=0}^{N_c-1} \lambda_3 f_3(k+j|k) \tag{19}$$

The objective functions of f_1 and f_2 can be normalized to achieve the same dimensions. f_1 can be divided into $(SoV_{max} - SoV_{min})^2$, where SoV_{max} and SoV_{min} are the upper and lower bounds of the SoV, and each component of f_2 can be divided by the maximum power loss of the related RC branch, as defined in (20).

$$P_{loss,max,R_0} = R_{0,max} i_{b,max}^2 \tag{20a}$$

$$P_{loss,max,R_1} = R_{1,max} i_{b,max}^2 \tag{20b}$$

$$P_{loss,max,R_2} = R_{2,max} i_{b,max}^2 \tag{20c}$$

where $R_{0,max}$, $R_{1,max}$, and $R_{2,max}$ are the maximum resistances of the battery cell model and $i_{b,max}$ is the maximum current of the cell, which is set to the C-rate. Given (18) and (20), after substituting and using I_b instead of i_b, the predicted total cost function of (19), can be represented by (21) over the prediction horizon.

$$J = \sum_{i=1}^{N_p} \frac{\lambda_1 (SoV_{ref} - SoV(k+i|k))^2}{(SoV_{max} - SoV_{min})^2}$$

$$+ \frac{\lambda_2}{I_{b,max}^2} \left(\frac{v_1^2(k+i|k)}{R_{1,max}R_1(SoC(k))} + \frac{v_2^2(k+i|k)}{R_{2,max}R_2(SoC(k))} \right.$$

$$\left. + \frac{R_0(SoC(k))I_b^2(k+i-1|k)}{R_{0,max}} \right)$$

$$+ \sum_{j=0}^{N_c-1} \lambda_3 \Delta I_b^2(k+j|k) \tag{21}$$

According to the state variables and battery and SC, the constraints of the optimization are presented in (22).

$$SoC_{min} \leq SoC(k) \leq SoC_{max}$$

$$v_{1,min} \leq v_1(k) \leq v_{1,max}$$

$$v_{2,min} \leq v_2(k) \leq v_{2,max}$$

$$SoV_{min} \leq SoV(k) \leq SoV_{max}$$

$$I_{b,min} \leq I_b(k) \leq I_{b,max} \tag{22}$$

Given the HESS state-space equations and inequality constraints, the inequality optimization problem is formulated

---

Algorithm 1 Hildreth's Quadratic Programming Algorithm

1: **Input:** H, f, M, b
2: **Output:** ΔU
3: Unconstrained solution $\Delta U = -H^{-1}f$
4: Check constraint satisfaction
5: **if** *constraints satisfy* **then**
    break
  else
    $P = MH^{-1}M^T, \quad D = MH^{-1}f + b$
  end
6: Initialize λ vectors
7: **while** $c <$ *max iterations* **do**
8:   **for** $i = 1 :$ *iterations number* **do**
9:   $\lambda_i^{c+1} = max(0, \frac{-1}{p_{ii}}[d_i + \sum_{j=1}^{i-1} p_{ij}\lambda_j^{c+1} + \sum_{j=i+1}^{n} p_{ij}\lambda_j^c])$

10:   **end for**
11: *count=count+1*
12: **end while**
13: **return** $\Delta U = -H^{-1}f - H^{-1}M^T\lambda$

---

in matrix form with state and control variables, which is provided by (23).

$$\min_{\Delta U(k)} \quad (R_s - X(k))^T \overline{Q(k)}(R_s - X(k))$$
$$+ \Delta U^T(k)\bar{R}\Delta U(k) \tag{23a}$$

subject to

$$x(k+i|k) = A(k+i-1|k)x(k+i-1|k) \tag{23b}$$
$$+ B(k+i-1|k)\Delta u(k+j|k)$$
$$+ B_d(k+i-1|k)P_L(k+i-1|k)$$

$$x_{min} \leq x(k+i+1|k) \leq x_{max} \tag{23c}$$

$$\Delta u_{min} \leq \Delta u(k+j|k) \leq \Delta u_{max} \tag{23d}$$

$$i \in \{1, 2, \ldots, N_p\}, \tag{23e}$$

$$j \in \{0, 1, \ldots, N_c - 1\} \tag{23f}$$

$$R_s = [r^T, r^T, \ldots, r^T]^T \in \mathbb{R}^{n_x N_p} \tag{23g}$$

$$r = [0, 0, 0, SoV_{ref}, 0]^T \in \mathbb{R}^{n_x} \tag{23h}$$

$$\overline{Q(k)} = diag(Q(k), \ldots, Q(k)) \in \mathbb{R}^{n_x N_p \times n_x N_p} \tag{23i}$$

$$Q(k) = diag\left(0, \frac{\lambda_2}{R_1(SoC(k))R_{1,max}I_{b,max}^2},\right.$$
$$\frac{\lambda_2}{R_2(SoC(k))R_{2,max}I_{b,max}^2}, \frac{\lambda_1}{(SoV_{max} - SoV_{min})^2},$$
$$\left.\frac{\lambda_2 R_0(SoC(k))}{R_{0,max}I_{b,max}^2}\right) \in \mathbb{R}^{n_x \times n_x} \tag{23j}$$

$$\bar{R} = diag(R, \ldots, R) \in \mathbb{R}^{n_u N_c \times n_u N_c} \tag{23k}$$

$$R = \lambda_3 \tag{23l}$$

where R_s is the reference trajectory or vector of the set point information for SoV over the prediction horizon, which includes SoV_{ref}; $\overline{Q(k)}$ and $\bar{R}$ are the weighting matrices of

the state and control variables, respectively; x_{max} and x_{min}; and Δu_{max} and Δu_{min} are the upper and lower bounds of the state and control variables, respectively. The control problem in (23) can be rewritten as a QP optimization problem, as defined in (24).

$$\min_{\Delta U(k)} \quad \frac{1}{2}\Delta U^T(k)H(k)\Delta U(k) + \Delta U^T(k)f(k) \tag{24a}$$

subject to $\quad M(k)\Delta U(k) \leq b(k) \tag{24b}$

$$H(k) = [\phi^T(k)\overline{Q(k)}\phi(k) + \bar{R}] \quad \in \mathbb{R}^{n_u N_c \times n_u N_c} \tag{24c}$$

$$f(k) = \phi^T(k)\overline{Q(k)}[F(k)x(k) - \phi_d(k)P_{L(ref)} - R_s] \in \mathbb{R}^{n_u N_c} \tag{24d}$$

$$M(k) = \begin{bmatrix} \phi(k) \\ -\phi(k) \end{bmatrix} \in \mathbb{R}^{2n_x N_p \times n_u N_c} \tag{24e}$$

$$b(k) = \begin{bmatrix} X_{max} - F(k)x(k) - \phi_d(k)P_{L(ref)}(k) \\ -X_{min} + F(k)x(k) + \phi_d(k)P_{L(ref)}(k) \end{bmatrix} \in \mathbb{R}^{2n_x N_p} \tag{24f}$$

$$X_{max} = \begin{bmatrix} x_{max} \\ \vdots \\ x_{max} \end{bmatrix}, \quad X_{min} = \begin{bmatrix} x_{min} \\ \vdots \\ x_{min} \end{bmatrix} \in \mathbb{R}^{n_x N_p} \tag{24g}$$

where $H(k)$ is the Hessian matrix, $f(k)$ is the vector of the coefficient, $M(k)$ is the matrix representing the linear constraints, and $b(k)$ is the vector on the right-hand side of the linear constraints. The inequality-constrained QP optimization problem in (24) can be solved using Hildreth's quadratic programming method, which is an iterative algorithm aimed at finding a solution to QP problems [60]. A general form of Hildreth's method is described by Algorithm 1, where the unconstrained solution is obtained and the final solution is calculated by iteration, considering the constraints imposed on all future state and control variables. Given the receding horizon control law, after computing the vector $\Delta U(k)$, only the first element of the control movement $\Delta u(k)$, is implemented in the system.

E. SUPERCAPACITOR VOLTAGE CONTROL STRATEGY

In this study, the control of the SoV is based on the EV's upcoming acceleration. In [34] and [31], SoV_{ref} was set at a fixed value of 0.75; in [61], it is determined by the EV's current speed; and in [21], it is computed based on the energy demand during braking. In this study, the value of SoV_{ref} is equal to SoV_{max}, which is set to 1. However, the SoV does not always follow SoV_{ref} because the weighting factor λ_1 changes based on the upcoming acceleration of the EV. It is assumed that the speed at the next time-step $(k + 1)$ is known. Thus, the EV's upcoming acceleration, $\bar{a}$, is defined in (25).

$$\bar{a} = (V_{EV}(k+1|k) - V_{EV}(k|k))/T \tag{25}$$

where $V_{EV}(k|k)$ is the current speed, and $V_{EV}(k + 1|k)$ is the upcoming speed at the next time-step. In the proposed
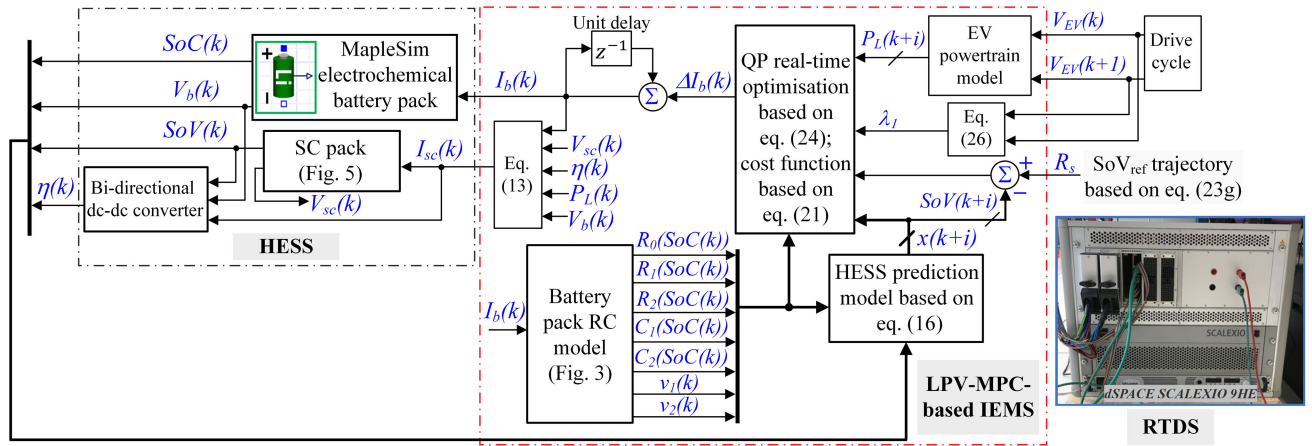
FIGURE 6. Block diagrams of the EV model and the LPV-MPC-based IEMS implemented in the RTDS.

strategy, λ_1 changes according to $\bar{a}$, by using (26).

$$\lambda_1 = \begin{cases} 1, & \text{if } \bar{a} \geq 0 \\ 0, & \text{otherwise.} \end{cases} \qquad (26)$$

As an EV is close to increasing its speed, it is essential to have SC adequately charged before the EV requests a significant amount of power [21]. In acceleration mode, the power demand is positive, causing the SC to discharge rapidly, resulting in voltage reduction. Consequently, it is essential to prevent the SC from fully discharging and maintaining its SoV at a high level. Similarly, during vehicle idling, the SC should be sufficiently charged by the battery to deliver the required power at the start time. Therefore, when $\bar{a} > 0$ or $\bar{a} = 0$, λ_1 is set to 1, leading to $SoV \rightarrow SoV_{ref}$, which is set to SoV_{max}. This method ensures that the SC is prevented from fast discharging and is charged to its maximum voltage, enabling it to be ready for efficient peak power delivery. Conversely, when the speed decreases, λ_1 is set to 0, allowing the SoV to vary freely. This enables the SC to supply power efficiently or to capture the energy produced by regenerative braking. Despite the simplicity of the proposed technique for controlling the SC voltage, it demonstrates outstanding performance in reducing battery current fluctuations as well as battery capacity and energy loss, outperforming other EMSs.

IV. REAL-TIME VALIDATION AND COMPARISON
A. IMPLEMENTATION CONFIGURATION
The proposed LPV-MPC-based IEMS is simulated in MAT-LAB/Simulink, and implemented in the RTDS along with the HESS model and the electrochemical battery cell. As shown in Fig. 6, to achieve more realistic results the electrochemical battery cell of MapleSim serves as a high-fidelity model for generating battery voltage and SoC. The RTDS is a dSPACE SCALAXIO 9HE processor with an Intel Xeon E4-1275 V3 CPU. Two drive cycles of the Worldwide Harmonized Light Vehicles Test Cycle (WLTC) class 2 and
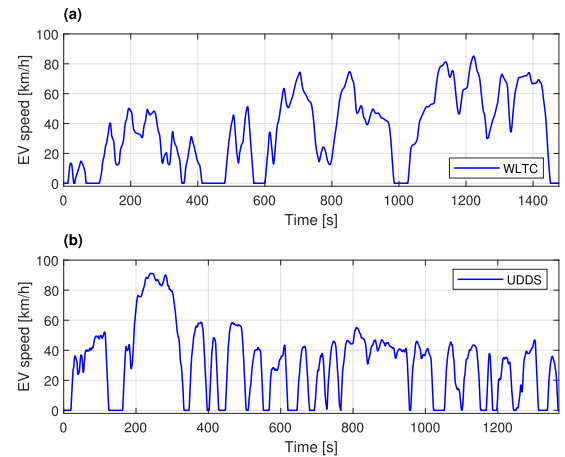

FIGURE 7. Speed drive cycles. (a) WLTC class 2. (b) UDDS (FTP-72).

the Urban Dynamometer Driving Schedule (UDDS) or the FTP-72 were selected as speed profiles, as shown in Fig. 7. Power demand is computed based on the drive cycle and EV powertrain model (B-class hatchback electric RWD), as presented in [45]. The LPV-MPC solves the QP optimization problem and determines the increment of the control variable for future N_c steps, whose first element, $\Delta u(k)$, is selected as the optimal value, which is the increment of the battery current. After computing $\Delta I_b(k)$, the values of $I_b(k)$ and $I_{sc}(k)$ are obtained, which in turn determine $SoV(k)$, $\eta(k)$, and RC model parameters. In addition, the MapleSim electrochemical model provides $V_b(k)$ and $SoC(k)$. The parameters of the HESS vary at each time-step, updating the state-space matrices, and this cycle continues.

B. HESS CHARACTERISTICS
The parameters of the battery cell RC model were extracted based on the specifications of the NCR18650B battery, as described in TABLE 1. To estimate the RC model parameters, the MapleSim electrochemical model of the

TABLE 1. Battery cell specifications [44].

Parameters	Value
Nominal Capacity at 0.2C-rate	3.25 Ah
Nominal Voltage	3.6 V
Upper cut-off voltage (SoC=1)	4.185 V
Lower cut-off voltage	2.5 V
Gravimetric Energy Density	251 Wh/kg
Mass(max)	46.5 g
Cathode material	$LiNi_{0.8}Co_{0.15}Al_{0.05}O_2$
Anode material	$Graphite-LiC_6$

TABLE 2. Supercapacitor cell specifications [57].

Parameters	Value
Rated Capacitance (C_{sc})	3000 F
Rated voltage ($v_{sc,r}$)	2.7 V
Absolute Maximum Current	2300 A
Gravimetric Specific Energy	6.4 Wh/kg
Stored Energy	3.04 Wh
Mass	475 g
Leakage current at 25°C	5 mA

TABLE 3. Parameters of the supercapacitor cell Faranda model [57].

R_s	R_f	R_{dis}	C_f	C_s	$2C_v$
1.92 Ω	0.36 $m\Omega$	540 Ω	2100 F	172 F	623 F/V

battery cell was used as the high-fidelity model. The parameters were calculated by measuring the cell terminal voltage using the discharge pulse current method during the relaxation time [44]. The pulse amplitude was set to the cell C-rate (3.25 A), and its duration was 72 s, causing the SoC to decrease by 2% for each pulse. Once the voltage curve was obtained, a curve-fitting method was applied to calculate the parameters for each SoC value. Subsequently, another curve-fitting method was applied to represent the RC parameters versus SoC. The accuracy of the obtained model was verified by implementation in the RTDS, resulting in an error of 0.052% in the root mean square percentage error (RMSPE) of the terminal voltage, as compared to the MapleSim electrochemical model [44]. The number of series and parallel arrays of the battery pack is 100 and 30, respectively. Hence, the total energy of the battery pack when it is fully charged (SoC=1) is 40.8 kWh, which is similar to that of the 2023 Nissan LEAF S with a battery pack capacity of 40 kWh. The parameters of the SC dynamic model are based on the characteristics of SC Maxwell BCAP3000, 3000F, 2.7V, whose parameters are listed in TABLE 2. The parameters of the SC model are obtained by a single fast current-controlled charge/discharge test, where a constant current charges the SC to its rated voltage, and then it is left to rest. Using the measured voltage and current data, the parameters were computed, as listed in TABLE 3, and the accuracy of the SC model was demonstrated [57]. The number of series and parallel SC cells is 50 and 1, respectively. Given the cell mass and specific energy, the total energy capacity of the SC pack is 0.152 kWh.
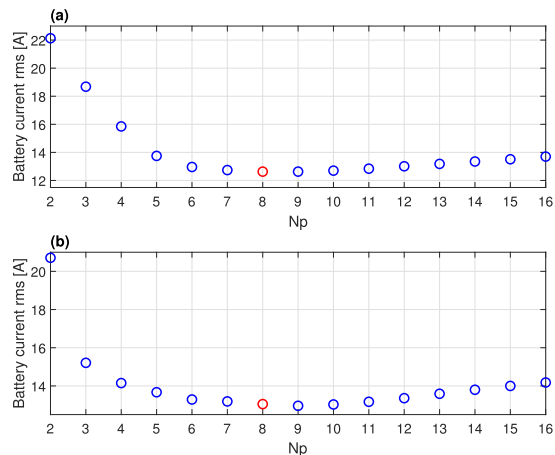
FIGURE 8. RMS of the battery current versus the prediction horizon under two drive cycles. (a) WLTC. (b) UDDS.

C. LPV-MPC PARAMETERS

The LPV-MPC and the QP optimization problem are self-coded using the MATLAB function block. This function can be employed to generate the C-code through a Simulink coder and an embedded coder for implementation in the RTDS. In the LPV-MPC, the discrete sample time, T, is set to 1 s, similar to that in [25], [34], and the simulation time-step is set as 200 ms. The prediction horizon and control horizon are both set to be equal and defined according to the RMS of the battery pack current, $I_{b,rms}$, as given in (27).

$$I_{b,rms} = \sqrt{\frac{1}{T_{end}} \int_0^{T_{end}} I_b^2(t)dt} \qquad (27)$$

where T_{end} denotes the drive cycle duration. Fig. 8 shows the relationship between $I_{b,rms}$ and N_p. A smaller prediction horizon leads to higher $I_{b,rms}$, whereas $I_{b,rms}$ gradually decreases with increasing in N_p. At $N_p = 8$, $I_{b,rms}$ reaches its optimum value. Because the anticipated power demand is known only at the next prediction time-step with a large N_p, there is a significant error between the actual and anticipated power demand. Moreover, a larger N_p imposes a heavier computational burden without significantly reducing the cost function [34], [62]. Therefore, the prediction horizon and control horizon are set to 8, resulting in smaller $I_{b,rms}$. According to λ_1 defined in (26), the value of λ_2 is set to 1 so that f_1 and f_2 have the same weight, and the weighting factor λ_3 is set to 0.02, to minimize $I_{b,rms}$. In the optimization problem, SoC_{min} and SoC_{max} are set to 0.2 and 1, respectively, and the cell maximum charge and discharge currents are set to 0.5 and 1 C-rate (3.25 A), respectively. Since the RC model capacitors can be fully discharged, the $v_{1,min}$ and $v_{2,min}$ are set to 0, and $v_{1,max}$ and $v_{2,max}$ are set to the maximum voltage of the cell which is 4.185 V. For the SC, SoV_{min} and SoV_{max} are set to 0.5 and 1, respectively. The initial SoC and SoV are set to 0.9. After implementing the HESS model and IEMS in the RTDS, the computation times in milliseconds [ms] for both drive cycles are shown in Fig. 9. It is evident that
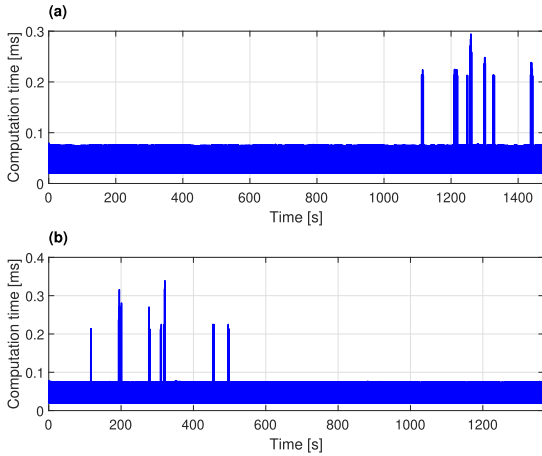
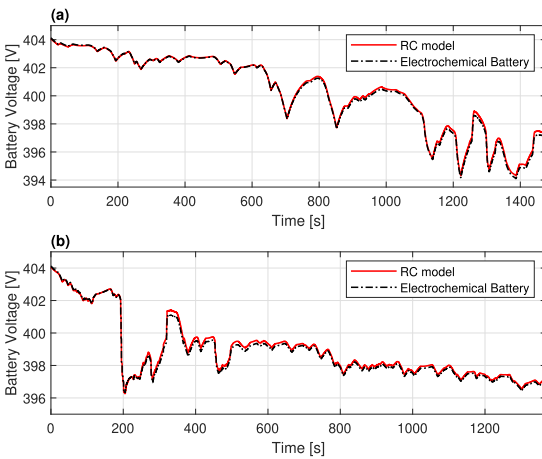**FIGURE 9.** Computation time in the RTDS under (a) WLTC. (b) UDDS.

FIGURE 10. Voltage of the battery pack RC model and electrochemical model in MapleSim. (a) WLTC. (b) UDDS.

FIGURE 11. Currents of (a) the Battery pack and (b) the SC pack under WLTC.

FIGURE 12. Currents of the (a) Battery pack and (b) the SC pack under UDDS.
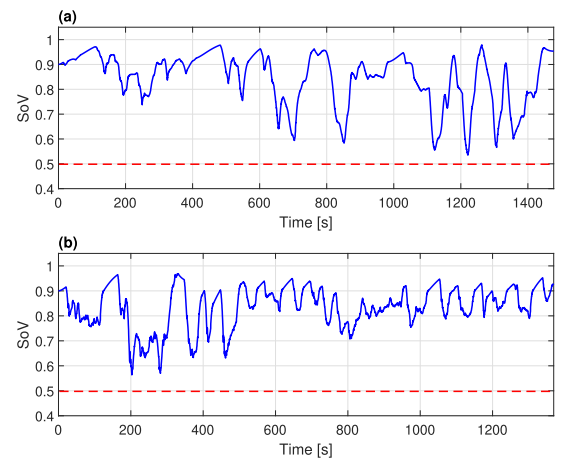
FIGURE 13. State-of-Voltage (SoV) under both drive cycles (a) WLTC. (b) UDDS.

this time is significantly shorter than the simulation time-step (200 ms). The terminal voltages of the RC model and the electrochemical model of the battery in MapleSim under the WLTC are depicted in Fig. 10(a), and those under the UDDS are shown in Fig.10(b). The electrochemical and RC models closely resemble each other, with the error for both drive cycles being 0.03%. Thus, the RC model is sufficiently accurate for use as an LPV model. The battery pack and SC pack currents under the WLTC are shown in Fig. 11, and those under UDDS drive cycles are shown in Fig. 12. It is evident that the fluctuations in the battery pack current are smaller than those in the SC pack current, and the battery current constraint is satisfied. The SoV of the SC for both drive cycles is shown in Fig. 13. In both cases, the SoV is consistently greater than 0.5 and varies based on the power demand and λ_1, which depends on the upcoming acceleration.

To conduct a precise analysis, a detailed view of the speed, λ_1, power flows, and SoV for the WLTC and UDDS drive cycles are presented in Fig. 14 and 15, respectively. Under the WLTC in Fig. 14, from 1222 s to 1262 s, the speed decreases. Therefore, according to (26), $\lambda_1 = 0$, and there is no control
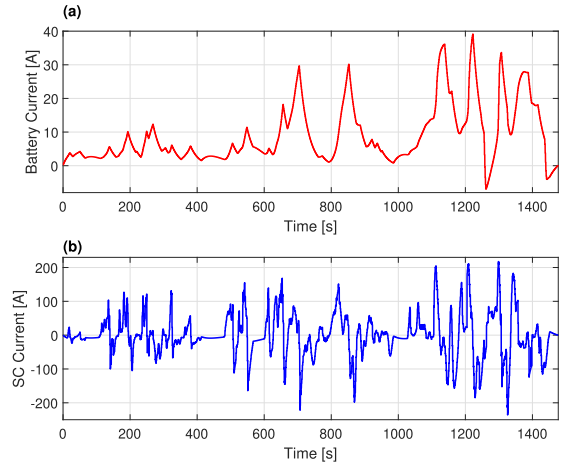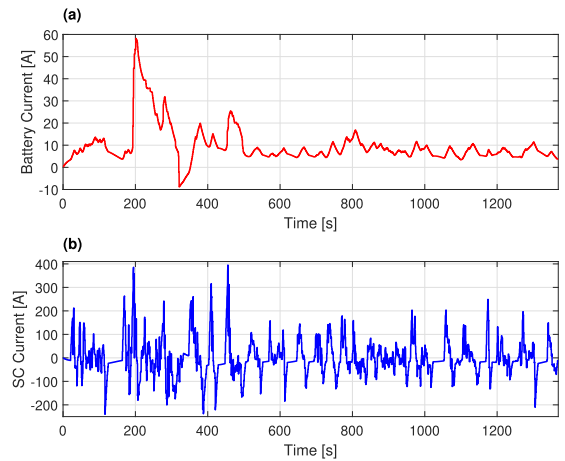
over the SoV. Initially, the power demand is positive, but the SC power flow is negative. Hence, the SC captures the energy produced during braking. Subsequently, at 1262 s,
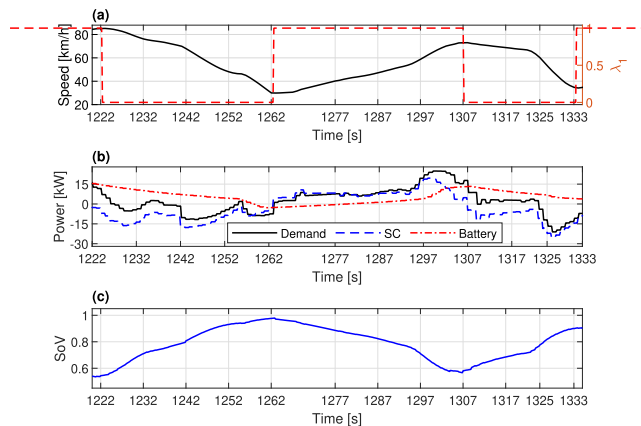
FIGURE 14. Results under WLTC drive cycle for (a) EV's speed and λ_1, (b) Power flows, and (c) SoV.

FIGURE 15. Results under UDDS drive cycle for (a) EV's speed and λ_1, (b) Power flows, and (c) SoV.

the speed increased, leading $\lambda_1 = 1$. The power demand is positive, necessitating that the SC supply the required power and assist the battery. Thus, from 1262 to 1307 s, the SC is under discharge and provides energy, leading to a reduction in the SoV. Note that λ_1 is set to 1 to prevent the SC from being completely and quickly discharged. Similarly, from 1307 to 1333 s, the speed decreases, and the power demand becomes negative. Consequently, the supercapacitor is charged and stores energy during regenerative braking.

Referring to Fig. 15, under the UDDS, when the speed decreases (for t in the range of 112 s to 125 s), $\lambda_1 = 0$ and there is no control over the SoV. However, following the cost function for minimizing the battery current stress and taking into account the negative power demand, the SoV increases. This means that the SC captures energy during regenerative braking and is charged. Subsequently, between 125 s and 163 s, when the EV is in idling mode and upcoming acceleration is zero (resulting in zero power demand), λ_1 is set to 1. During this time frame, the SC is charged by the battery ($SoV \rightarrow 1$) to deliver the required power when the EV starts to move. Then, from 163 to 172 s, the speed begins to increase, and λ_1 is still 1. However, the power demand becomes positive. During this period, the SoV decreases as the SC assists the battery in supplying the required power. Similarly, from 172 s onwards, the speed decreases, and λ_1 becomes 0; the SC is recharged owing to the negative power demand of regenerative braking. This charging and discharging cycle of the SC continues throughout the entire route.

D. COMPARISON TO OTHER METHODS
The performance of the proposed LPV-MPC-based IEMS was assessed through a comparison with various EMSs based on five evaluation factors: the battery pack RMS and peak current, battery ampere-hour throughput, capacity loss of the battery cell, and energy loss of the battery pack. These factors have been widely used for evaluating battery degradation in EV applications [10], [33], [34], [40], [41], [42]. The
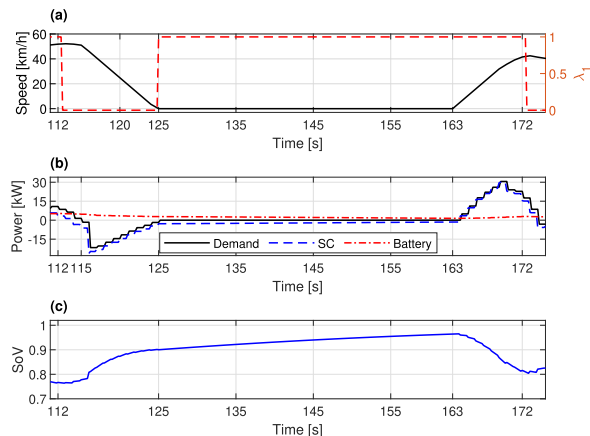
RMS current of the battery pack, defined in (27), is the most important factor for evaluating battery degradation. Moreover, the battery cell capacity loss Q_{loss}, as defined in (28), is a commonly adopted approach for evaluating the battery lifespan [34], [40], [41], which is a semi-empirical technique based on the Arrhenius degradation model [41].

$$Q_{loss} = A \cdot exp(\frac{E_a + B \cdot C_{rate}}{R \cdot T_{bat}}) \cdot (A_h)^z \qquad (28)$$

where A is the pre-exponential factor, C_{rate} is the discharge/charge rate, B is the compensation factor at C-rate, R is the gas constant, T_{bat} is the absolute temperature, A_h is the Ampere-hour throughput, and z is the time factor [41]. The factor of the battery ampere-hour throughput from t_0 to t is defined in (29), which was also utilized in [10] and [33] to evaluate the performance of the MPC in battery degradation.

$$A_h = \frac{1}{3600} \int_{t_0}^{t} |I_b(t)| dt \qquad (29)$$

Another factor for evaluating the battery degradation, which is used in [34], is the energy loss of the battery pack, as defined in (30).

$$E_{loss} = \int_{t_0}^{t} P_{loss}(t) dt \qquad (30)$$

The EMSs are verified under two drive cycles of the WLTC and UDDS. Their results are provided in TABLE 4, where the first method used for comparison is the LPV-MPC method of [34], in which $SoV_{ref} = 0.75$, and for a meaningful comparison, the power demand prediction at the next time-step is taken into account. The second method is the LTI-MPC, which utilizes a fixed state-space model and $SoV_{ref} = 0.75$. The third method is the LPV-MPC, in which the SoV_{ref} varies based on the current speed, according to the method presented in [61], using $\sqrt{1 - V_{EV}/V_{EV,max}}$, where V_{EV} and $V_{EV,max}$ are the EV's current and maximum speed, respectively. The fourth and fifth methods are filter-based [45] and deterministic rule-based methods [13]. Given TABLE 4 under both drive cycles,

TABLE 4. Comparison of different EMSs on battery degradation under two drive cycles.

Drive cycle	Energy management strategy	RMS current $I_{b,rms}$ [A]	Discharge peak I_b [A]	Charge peak I_b [A]	Ah throughput of battery [Ah]	Capacity loss $Q_{loss} \times 10^{-4}$ [%]	Energy loss [kJ]
WLTC	Proposed LPV-MPC	12.46	39.12	6.97	3.754	1.274	33.41
	LPV-MPC in [34]	15.35	56.10	9.40	4.158	1.338	47.10
	LPV-MPC, SoV control by [61]	14.35	61.93	6.65	3.790	1.349	41.13
	LTI-MPC	16.13	51.39	19.04	4.645	1.514	48.23
	Filter-based strategy	15.47	49.74	17.35	4.397	1.442	37.51
	Rule-based strategy	19.08	63.75	43.20	5.364	1.708	57.06
UDDS	Proposed LPV-MPC	12.90	58.18	8.80	3.773	1.309	33.69
	LPV-MPC in [34]	14.78	83.54	12.93	3.945	1.356	41.71
	LPV-MPC, SoV control by [61]	13.91	72.72	15.40	3.846	1.342	37.77
	LTI-MPC	17.23	83.15	19.47	4.817	1.533	50.30
	Filter-based strategy	16.45	75.95	25.37	4.546	1.468	39.37
	Rule-based strategy	20.11	83.91	42.64	5.128	1.646	58.84

for the proposed LPV-MPC-based IEMS, the battery RMS current, discharge peak current, ampere-hour throughput, capacity loss, and energy loss of the battery were smaller than those of the other methods. Under the WLTC, in a comparison with [34], $I_{b,rms}$ is reduced by up to 18.82%, and the discharge and charge peak currents are reduced by up to 30.26% and 25.85%, respectively. Moreover, the ampere-hour throughput, capacity loss, and energy loss of the battery are reduced 9.71%, 4.78%, and 29.06%, respectively. Similarly, under the UDDS drive cycle, the proposed LPV-MPC-based IEMS maintains its superiority by reducing $I_{b,rms}$, discharge and charge peak currents, ampere-hour throughput, and capacity and energy losses to 12.71%, 30.35%, 31.94%, 4.35%, 3.46%, and 19.22%, respectively. This result demonstrates that considering the upcoming speed in the LPV-MPC leads to a lower RMS current and battery capacity loss, thereby contributing to a more efficient battery lifespan compared to other methods. This remarkable performance is primarily attributed to the utilization of the LPV model for the HESS and the introduction of the new SoV control strategy based on the expected acceleration of the EV.

V. CONCLUSION

In this study, an LPV-MPC-based IEMS is developed to split the load power between the battery and SC packs, while also extending the battery lifetime. The dynamic model of the battery is used to develop the prediction model within the LPV-MPC framework. The state-space model matrices are updated at each time-step based on the SoC and SoV of the battery and the SC, respectively. The control issue is transformed into an inequality-constrained QP optimization problem, which is implemented in the RTDS. The proposed approach incorporates upcoming acceleration into SoV control, effectively enhancing SC utilization and reducing battery current stress. The proposed method was compared with various EMSs by measuring the RMS current, peak current, ampere-hour throughput, capacity loss of the battery cell, and energy loss of the battery pack. The substantial reductions observed in these evaluation factors demonstrate the superiority of the proposed IEMS in EV applications compared to others.

REFERENCES

[1] S. Habib, M. M. Khan, F. Abbas, L. Sang, M. U. Shahid, and H. Tang, "A comprehensive study of implemented international standards, technical challenges, impacts and prospects for electric vehicles," *IEEE Access*, vol. 6, pp. 13866–13890, 2018.

[2] J. Park, Y. L. Murphey, and M. A. Masrur, "Intelligent energy management and optimization in a hybridized all-terrain vehicle with simple on–off control of the internal combustion engine," *IEEE Trans. Veh. Technol.*, vol. 65, no. 6, pp. 4584–4596, Jun. 2016.

[3] A. K. Karmaker, M. A. Hossain, H. R. Pota, A. Onen, and J. Jung, "Energy management system for hybrid renewable energy-based electric vehicle charging station," *IEEE Access*, vol. 11, pp. 27793–27805, 2023.

[4] E. Schaltz, A. Khaligh, and P. O. Rasmussen, "Influence of battery/ultracapacitor energy-storage sizing on battery lifetime in a fuel cell hybrid electric vehicle," *IEEE Trans. Veh. Technol.*, vol. 58, no. 8, pp. 3882–3891, Oct. 2009.

[5] S. Pay and Y. Baghzouz, "Effectiveness of battery-supercapacitor combination in electric vehicles," in *Proc. IEEE Bologna Power Tech Conf.*, vol. 3, 2003, p. 6. [Online]. Available: https://ieeexplore.ieee.org/document/1304472

[6] X. Luo, J. V. Barreras, C. L. Chambon, B. Wu, and E. Batzelis, "Hybridizing lead–acid batteries with supercapacitors: A methodology," *Energies*, vol. 14, no. 2, p. 507, Jan. 2021.

[7] M. Uno and K. Tanaka, "Influence of high-frequency charge–discharge cycling induced by cell voltage equalizers on the life performance of lithium-ion cells," *IEEE Trans. Veh. Technol.*, vol. 60, no. 4, pp. 1505–1515, May 2011.

[8] Z. Song, H. Hofmann, J. Li, J. Hou, X. Han, and M. Ouyang, "Energy management strategies comparison for electric vehicles with hybrid energy storage system," *Appl. Energy*, vol. 134, pp. 321–331, Dec. 2014.

[9] T. Mesbahi, F. Khenfri, N. Rizoug, P. Bartholomeüs, and P. L. Moigne, "Combined optimal sizing and control of Li-ion battery/supercapacitor embedded power supply using hybrid particle Swarm–Nelder–Mead algorithm," *IEEE Trans. Sustain. Energy*, vol. 8, no. 1, pp. 59–73, Jan. 2017.

[10] X. Lu and H. Wang, "Optimal sizing and energy management for cost-effective PEV hybrid energy storage systems," *IEEE Trans. Ind. Informat.*, vol. 16, no. 5, pp. 3407–3416, May 2020.

[11] R. Ostadian, J. Ramoul, A. Biswas, and A. Emadi, "Intelligent energy management systems for electrified vehicles: Current status, challenges, and emerging trends," *IEEE Open J. Veh. Technol.*, vol. 1, pp. 279–295, 2020.

[12] A. K. Gautam, M. Tariq, J. P. Pandey, K. S. Verma, and S. Urooj, "Hybrid sources powered electric vehicle configuration and integrated optimal power management strategy," *IEEE Access*, vol. 10, pp. 121684–121711, 2022.

[13] J. P. Trovão, P. G. Pereirinha, H. M. Jorge, and C. H. Antunes, "A multi-level energy management system for multi-source electric vehicles—An integrated rule-based meta-heuristic approach," *Appl. Energy*, vol. 105, pp. 304–318, May 2013.

[14] B. Wang, J. Xu, B. Cao, and X. Zhou, "A novel multimode hybrid energy storage system and its energy management strategy for electric vehicles," *J. Power Sources*, vol. 281, pp. 432–443, May 2015.

[15] Y. Liu, Z. Yang, X. Wu, D. Sha, F. Lin, and X. Fang, "An adaptive energy management strategy of stationary hybrid energy storage system," *IEEE Trans. Transport. Electrific.*, vol. 8, no. 2, pp. 2261–2272, Jun. 2022.

[16] H. Yin, W. Zhou, M. Li, C. Ma, and C. Zhao, "An adaptive fuzzy logic-based energy management strategy on battery/ultracapacitor hybrid electric vehicles," *IEEE Trans. Transport. Electrific.*, vol. 2, no. 3, pp. 300–311, Sep. 2016.

[17] Q. Zhang, F. Ju, S. Zhang, W. Deng, J. Wu, and C. Gao, "Power management for hybrid energy storage system of electric vehicles considering inaccurate terrain information," *IEEE Trans. Autom. Sci. Eng.*, vol. 14, no. 2, pp. 608–618, Apr. 2017.

[18] L. Sun, K. Feng, C. Chapman, and N. Zhang, "An adaptive power-split strategy for battery–supercapacitor powertrain—Design, simulation, and experiment," *IEEE Trans. Power Electron.*, vol. 32, no. 12, pp. 9364–9375, Dec. 2017.

[19] O. Salari, K. Hashtrudi-Zaad, A. Bakhshai, M. Z. Youssef, and P. Jain, "A systematic approach for the design of the digital low-pass filters for energy storage systems in EV applications," *IEEE J. Emerg. Sel. Topics Ind. Electron.*, vol. 1, no. 1, pp. 67–79, Jul. 2020.

[20] C. Chang, W. Zhao, C. Wang, and Y. Song, "A novel energy management strategy integrating deep reinforcement learning and rule based on condition identification," *IEEE Trans. Veh. Technol.*, vol. 72, no. 2, pp. 1674–1688, Feb. 2023.

[21] M.-E. Choi, J.-S. Lee, and S.-W. Seo, "Real-time optimization for power management systems of a battery/supercapacitor hybrid energy storage system in electric vehicles," *IEEE Trans. Veh. Technol.*, vol. 63, no. 8, pp. 3600–3611, Oct. 2014.

[22] C. M. Martinez, X. Hu, D. Cao, E. Velenis, B. Gao, and M. Wellers, "Energy management in plug-in hybrid electric vehicles: Recent progress and a connected vehicles perspective," *IEEE Trans. Veh. Technol.*, vol. 66, no. 6, pp. 4534–4549, Jun. 2017.

[23] Z. Chen, C. C. Mi, J. Xu, X. Gong, and C. You, "Energy management for a power-split plug-in hybrid electric vehicle based on dynamic programming and neural networks," *IEEE Trans. Veh. Technol.*, vol. 63, no. 4, pp. 1567–1580, May 2014.

[24] F. R. Salmasi, "Control strategies for hybrid electric vehicles: Evolution, classification, comparison, and future trends," *IEEE Trans. Veh. Technol.*, vol. 56, no. 5, pp. 2393–2404, Sep. 2007.

[25] B.-H. Nguyen, T. Vo-Duy, M. C. Ta, and J. P. F. Trovão, "Optimal energy management of hybrid storage systems using an alternative approach of Pontryagin's minimum principle," *IEEE Trans. Transp. Electrific.*, vol. 7, no. 4, pp. 2224–2237, Dec. 2021.

[26] F. Odeim, J. Roes, and A. Heinzel, "Power management optimization of a fuel cell/battery/supercapacitor hybrid system for transit bus applications," *IEEE Trans. Veh. Technol.*, vol. 65, no. 7, pp. 5783–5788, Jul. 2016.

[27] A. Biswas and A. Emadi, "Energy management systems for electrified powertrains: State-of-the-art review and future trends," *IEEE Trans. Veh. Technol.*, vol. 68, no. 7, pp. 6453–6467, Jul. 2019.

[28] F. Xu and T. Shen, "Look-ahead prediction-based real-time optimal energy management for connected HEVs," *IEEE Trans. Veh. Technol.*, vol. 69, no. 3, pp. 2537–2551, Mar. 2020.

[29] Q. Li, P. Liu, X. Meng, G. Zhang, Y. Ai, and W. Chen, "Model prediction control-based energy management combining self-trending prediction and subset-searching algorithm for hydrogen electric multiple unit train," *IEEE Trans. Transp. Electrific.*, vol. 8, no. 2, pp. 2249–2260, Jun. 2022.

[30] X. Liu, Y. Suo, Z. Zhang, X. Song, and J. Zhou, "A new model predictive current control strategy for hybrid energy storage system considering the SOC of the supercapacitor," *IEEE J. Emerg. Sel. Topics Power Electron.*, vol. 11, no. 1, pp. 325–338, Feb. 2023.

[31] P. Golchoubian and N. L. Azad, "Real-time nonlinear model predictive control of a battery–supercapacitor hybrid energy storage system in electric vehicles," *IEEE Trans. Veh. Technol.*, vol. 66, no. 11, pp. 9678–9688, Nov. 2017.

[32] B. Hredzak, V. G. Agelidis, and G. Demetriades, "Application of explicit model predictive control to a hybrid battery-ultracapacitor power source," *J. Power Sources*, vol. 277, pp. 84–94, Mar. 2015. [Online]. Available: https://www.sciencedirect.com/science/article/pii/S0378775314020151

[33] L. Wang, Y. Wang, C. Liu, D. Yang, and Z. Chen, "A power distribution strategy for hybrid energy storage system using adaptive model predictive control," *IEEE Trans. Power Electron.*, vol. 35, no. 6, pp. 5897–5906, Jun. 2020.

[34] C. Jia, J. Cui, W. Qiao, and L. Qu, "Real-time model predictive control for battery-supercapacitor hybrid energy storage systems using linear parameter-varying models," *IEEE J. Emerg. Sel. Topics Power Electron.*, vol. 11, no. 1, pp. 251–263, Feb. 2023.

[35] A. Taghavipour and S. Moghadasi, "A real-time nonlinear CRPE predictive PHEV energy management system design and HIL evaluation," *IEEE Trans. Veh. Technol.*, vol. 70, no. 1, pp. 49–58, Jan. 2021.

[36] F. Zhou, F. Xiao, C. Chang, Y. Shao, and C. Song, "Adaptive model predictive control-based energy management for semi-active hybrid energy storage systems on electric vehicles," *Energies*, vol. 10, no. 7, p. 1063, Jul. 2017. [Online]. Available: https://www.mdpi.com/1996-1073/10/7/1063

[37] H. Wang, Y. Huang, H. He, C. Lv, W. Liu, and A. Khajepour, "Energy management of hybrid electric vehicles," in *Modeling, Dynamics and Control of Electrified Vehicles*, H. Zhang, D. Cao, and H. Du, Eds. Bedford, U.K.: Cranfield Univ., 2018, ch. 5, pp. 159–206. [Online]. Available: https://www.sciencedirect.com/science/article/abs/pii/B9780128127865000057

[38] S. D. Cairano, D. Bernardini, A. Bemporad, and I. V. Kolmanovsky, "Stochastic MPC with learning for driver-predictive vehicle control and its application to HEV energy management," *IEEE Trans. Control Syst. Technol.*, vol. 22, no. 3, pp. 1018–1031, May 2014.

[39] M. R. Larijani, M. Zolghadri, S. H. Kia, and A. El Hajjaji, "Performance analysis of the lithium-ion battery RC equivalent circuit model using EPA drive cycles," in *Proc. 13th Power Electron., Drive Syst., Technol. Conf. (PEDSTC)*, Feb. 2022, pp. 393–397.

[40] Q. Zhang and G. Li, "Experimental study on a semi-active battery-supercapacitor hybrid energy storage system for electric vehicle application," *IEEE Trans. Power Electron.*, vol. 35, no. 1, pp. 1014–1021, Jan. 2020.

[41] Z. Song, J. Li, X. Han, L. Xu, L. Lu, M. Ouyang, and H. Hofmann, "Multi-objective optimization of a semi-active battery/supercapacitor energy storage system for electric vehicles," *Appl. Energy*, vol. 135, pp. 212–224, Dec. 2014. [Online]. Available: https://www.sciencedirect.com/science/article/pii/S0306261914008964

[42] L. Timilsina, P. R. Badr, P. H. Hoang, G. Ozkan, B. Papari, and C. S. Edrington, "Battery degradation in electric and hybrid electric vehicles: A survey study," *IEEE Access*, vol. 11, pp. 42431–42462, 2023.

[43] C. Jia, W. Qiao, J. Cui, and L. Qu, "Adaptive model-predictive-control-based real-time energy management of fuel cell hybrid electric vehicles," *IEEE Trans. Power Electron.*, vol. 38, no. 2, pp. 2681–2694, Feb. 2023.

[44] M. R. Larijani, M. Zolghadri, S. H. Kia, and A. El Hajjaji, "Battery cell dynamic modeling using the RC equivalent circuit for RTDS frameworks," in *Proc. 47th Annu. Conf. IEEE Ind. Electron. Soc. (IECON)*, Oct. 2021, pp. 1–6.

[45] M. R. Larijani, S. H. Kia, M. Zolghadri, A. El Hajjaji, and A. Taghavipour, "Modeling and controller design of battery/SC electric vehicles for real-time energy management," in *Proc. IEEE 97th Veh. Technol. Conf. (VTC-Spring)*, Jun. 2023, pp. 1–7.

[46] P. Bhattacharyya, A. Banerjee, S. Sen, S. K. Giri, and S. Sadhukhan, "A modified semi-active topology for battery-ultracapacitor hybrid energy storage system for EV applications," in *Proc. IEEE Int. Conf. Power Electron., Smart Grid Renew. Energy (PESGRE)*, Jan. 2020, pp. 1–6.

[47] B.-H. Nguyen, R. German, J. P. F. Trovão, and A. Bouscayrol, "Real-time energy management of battery/supercapacitor electric vehicles based on an adaptation of Pontryagin's minimum principle," *IEEE Trans. Veh. Technol.*, vol. 68, no. 1, pp. 203–212, Jan. 2019.

[48] Z. Yang, D. Patil, and B. Fahimi, "Electrothermal modeling of lithium-ion batteries for electric vehicles," *IEEE Trans. Veh. Technol.*, vol. 68, no. 1, pp. 170–179, Jan. 2019.

[49] H. Miniguano, A. Barrado, and A. Lázaro, "Li-ion battery and supercapacitor modeling for electric vehicles based on pulse—Pseudo random binary sequence," *IEEE Trans. Veh. Technol.*, vol. 70, no. 11, pp. 11378–11389, Nov. 2021.

[50] M. Adaikkappan and N. Sathiyamoorthy, "Modeling, state of charge estimation, and charging of lithium-ion battery in electric vehicle: A review," *Int. J. Energy Res.*, vol. 46, no. 3, pp. 2141–2165, Mar. 2022.

[51] L. Siguang and Z. Chengning, "Study on battery management system and lithium-ion battery," in *Proc. Int. Conf. Comput. Autom. Eng.*, Mar. 2009, pp. 218–222.

[52] R. R. Kumar, C. Bharatiraja, K. Udhayakumar, S. Devakirubakaran, K. S. Sekar, and L. Mihet-Popa, "Advances in batteries, battery modeling, battery management system, battery thermal management, SOC, SOH, and charge/discharge characteristics in EV applications," *IEEE Access*, vol. 11, pp. 105761–105809, 2023.

[53] M. Chen and G. A. Rincon-Mora, "Accurate electrical battery model capable of predicting runtime and I-V performance," *IEEE Trans. Energy Convers.*, vol. 21, no. 2, pp. 504–511, Jun. 2006.

[54] R. Faranda, M. Gallina, and D. T. Son, "A new simplified model of double-layer capacitors," in *Proc. Int. Conf. Clean Electr. Power*, May 2007, pp. 706–710.

[55] F. Naseri, E. Farjah, T. Ghanbari, Z. Kazemi, E. Schaltz, and J.-L. Schanen, "Online parameter estimation for supercapacitor state-of-energy and state-of-health determination in vehicular applications," *IEEE Trans. Ind. Electron.*, vol. 67, no. 9, pp. 7963–7972, Sep. 2020.

[56] L. Zubieta and R. Bonert, "Characterization of double-layer capacitors for power electronics applications," *IEEE Trans. Ind. Appl.*, vol. 36, no. 1, pp. 199–205, Jan. 2000.

[57] A. Lahyani, P. Venet, A. Guermazi, and A. Troudi, "Battery/supercapacitors combination in uninterruptible power supply (UPS)," *IEEE Trans. Power Electron.*, vol. 28, no. 4, pp. 1509–1522, Apr. 2013.

[58] M. M. Morato, J. E. Normey-Rico, and O. Sename, "Model predictive control design for linear parameter varying systems: A survey," *Annu. Rev. Control*, vol. 49, pp. 64–80, 2020. [Online]. Available: https://www.sciencedirect.com/science/article/pii/S1367578820300250

[59] E. Redondo-Iglesias, P. Venet, and S. Pelissier, "Modelling lithium-ion battery ageing in electric vehicle applications—Calendar and cycling ageing combination effects," *Batteries*, vol. 6, no. 1, p. 14, Feb. 2020. [Online]. Available: https://www.mdpi.com/2313-0105/6/1/14

[60] L. Wang, "Discrete-time MPC with constraints," in *Model Predictive Control System Design and Implementation Using MATLAB®*. London, U.K.: Springer, 2009, pp. 43–84.

[61] R. Carter, A. Cruden, and P. J. Hall, "Optimizing for efficiency or battery life in a battery/supercapacitor electric vehicle," *IEEE Trans. Veh. Technol.*, vol. 61, no. 4, pp. 1526–1533, May 2012.

[62] X. Hu, C. Zou, X. Tang, T. Liu, and L. Hu, "Cost-optimal energy management of hybrid electric vehicles using fuel cell/battery health-aware predictive control," *IEEE Trans. Power Electron.*, vol. 35, no. 1, pp. 382–392, Jan. 2020.

MORTEZA REZAEI LARIJANI (Student Member, IEEE) received the B.Sc. degree in electrical engineering from the Ferdowsi University of Mashhad, Mashhad, Iran, in 2013, and the M.Sc. degree in electrical engineering (power electronics and electrical machines) from the Sharif University of Technology, Tehran, Iran, in 2015. He is currently pursuing the cotutelle Ph.D. degree in electrical engineering with the Sharif University of Technology and the University of Picardie Jules Verne (UPJV), Amiens, France.

He is with the Modeling, Information and Systems Laboratory (MIS-UR4290). His research interests include real-time energy management in electric vehicles, power electronics, model predictive control, FPGA programming, and modeling and control of power electronic converters.

SHAHIN HEDAYATI KIA received the M.Sc. degree in electrical engineering from Iran University of Science and Technology, Tehran, Iran, in 1998, and the M.Sc. and Ph.D. degrees (Hons.) in power electrical engineering from the University of Picardie Jules Verne (UPJV), Amiens, France, in 2005 and 2009, respectively.

From 1998 to 2004, he worked for several Iranian companies, namely Pars Navard Engineering Company, AAlipayam Medical Engineering Company, Saameh Company, and ONA Company. From 2008 to 2009, he was a Lecturer with Institute Supérieur des Sciences et Techniques (INSSET), Saint-Quentin, France. From September 2009 to September 2011, he was a Postdoctoral Associate with the School of Electronic and Electrical Engineering of Amiens (ESIEE-Amiens), UPJV. He is currently an Associate Professor and a member of the Department of Electrical Engineering and the Modeling, Information and Systems Laboratory (MIS-UR4290).

MOHAMMADREZA ZOLGHADRI (Senior Member, IEEE) received the B.Sc. and M.Sc. degrees in electrical engineering from the Sharif University of Technology, Tehran, Iran, in 1989 and 1992, respectively, and the Ph.D. degree in electrical engineering from Institute National Polytechnique de Grenoble (INPG), Grenoble, France, in 1997.

In 1997, he joined the Department of Electrical Engineering, Sharif University of Technology. From 2000 to 2003, he was a Senior Researcher with the Electronics Laboratory, SAM Electronics Company, Tehran. From 2003 to 2005, he was a Visiting Professor with North Carolina A&T State University, USA. He is currently an Associate Professor and the Head of the Power System Group, Department of Electrical Engineering, Sharif University of Technology. He is also the Founder and the Head of the Electric Drives and Power Electronics Laboratory (EDPEL), Sharif University of Technology. He is the author of more than 100 publications in power electronics and variable speed drives. His research interests include the application of power electronics in energy systems, modeling, and control of power electronic converters and variable speed drives. He has been a member of the Founding Board of the Power Electronics Society of Iran (PELSI) and the Chairperson of the Board of PELSI, since February 2019.

AHMED EL HAJJAJI received the Ph.D. degree in automatic control and the H.D.R. degree from the University of Picardie Jules Verne (UPJV), France, in 1993 and 2000, respectively.

He was the Director of the Professional Institute of Electrical Engineering and Industrial Computing, from 2006 to 2012. He is currently a Full Professor and the Head of the Automatic Control and Vehicle Research Group, Modeling, Information and Systems Laboratory (MIS-UR4290), UPJV. Since 1994, he has published more than 350 journals and conference papers in the areas of advanced fuzzy control, fault detection, diagnosis, and fault tolerant control and their applications to vehicle dynamics, engine control, power systems, renewable energy conversion systems, and industrial processes. His research interests include fuzzy control, vehicle dynamics, fault-tolerant control, neural networks, maglev systems, and renewable energy conversion systems.

AMIR TAGHAVIPOUR received the B.Sc. and M.Sc. degrees in mechanical engineering from the Sharif University of Technology, Tehran, Iran, in 2007 and 2010, respectively, and the Ph.D. degree in the design and implementation of real-time optimal energy management systems for plug-in hybrid electric vehicles in collaboration with Toyota Technical Centre North America and MapleSoft Canada from the Systems Design Engineering Department, University of Waterloo, in 2014.

He is currently an Assistant Professor with the Department of Mechanical Engineering, K. N. Toosi University of Technology. His research interests include model-based and real-time controller design for mechatronic and sustainable energy systems, especially energy management systems for fully electric, hybrid (electric and hydraulic), plug-in hybrid, and fuel cell-powered vehicles. His research interests include intelligent hybrid and electric vehicles, automotive systems control, modeling and prototyping, model predictive control, nonlinear and hybrid systems, and optimization approaches.

• • •